

# Broadening the Atmospheric Bridge Paradigm: ENSO Teleconnections to the Tropical West Pacific-Indian Oceans Over the Seasonal Cycle and to the North Pacific in Summer

Michael A. Alexander

*NOAA-CIRES, Climate Diagnostics Center, Boulder, Colorado*

Ngar-Cheung Lau

*NOAA/Geophysical Fluid Dynamics Laboratory, Princeton, New Jersey*

James D. Scott

*NOAA-CIRES, Climate Diagnostics Center, Boulder, Colorado*

*Accepted as a chapter in the AGU Monograph Ocean-Atmosphere Interaction and Climate Variability*

*(March 2004)*

## ABSTRACT

During El Niño-Southern Oscillation (ENSO) events, atmospheric teleconnections associated with sea surface temperature (SST) anomalies in the equatorial Pacific can influence the ocean thousands of kilometers away. We use several data sets to delineate this “atmospheric bridge” between ocean basins, focusing on two emerging research areas: 1) the evolution of atmosphere-ocean interactions in the tropical Indian-Western Pacific Oceans over the full ENSO cycle and 2) the formation of large amplitude SST anomalies in North Pacific in the summer before ENSO peaks. In ENSO composites [where events peak near the end of Yr(0)], an east-west SST dipole develops in the Indian Ocean during the summer-fall of Yr(0), followed by basin-wide warming through spring of Yr(1). The SST anomalies over most of the tropical west Pacific also reverse sign, from negative in summer of Yr(0) to positive in the following summer. Local air-sea interactions influence the evolution of these ENSO-induced SST anomalies and related sea level pressure (SLP) and precipitation anomalies. Over the western North Pacific, the southward displacement of the jet stream and storm track in the summer of Yr(0) changes the solar radiation and latent heat flux at the surface, which results in anomalous cooling (and deepening) of the oceanic mixed layer at ~40°N. The potential impact of both the tropical and North Pacific SST anomalies on the broader climate is discussed.

## 1. INTRODUCTION

While the essential atmospheric and oceanic processes responsible for El Niño and the Southern Oscillation (ENSO) are contained within the tropical Pacific, ENSO impacts the global climate system. Some of the ENSO signal is communicated to remote locations via coastally trapped ocean waves that propagate poleward along the west coast of North and South America [Enfield and Allen, 1980; Pares-Sierra and O'Brien, 1989], but most of the teleconnections are through the atmosphere [Alexander 1992; Lau and Nath 1996, Alexander et al., 2002; Lau and Nath 2003]. The global atmospheric response to SST anomalies in the equatorial Pacific includes changes in the wind, temperature, moisture and cloud cover, which then alter the fluxes of heat, momentum and fresh water into the ocean. Through this “atmospheric bridge”, changes in the central and eastern equatorial Pacific Ocean are communicated to the global oceans via atmospheric teleconnections associated with ENSO.

In general, ENSO begins in boreal spring, peaks in late fall/early winter and decays in the following spring. In addition, the extratropical atmospheric circulation anomalies associated with ENSO are strongest in northern winter. As a result, most studies of the atmospheric bridge have focused on boreal winter through the following spring. The roughly one season lag in the SST response to the atmospheric forcing is due to the large thermal inertia of the ocean. However, significant bridge-related changes in the climate system also occur in other seasons, including both the previous and following summers.

The evolution of the atmospheric bridge is illustrated in Plate 1 by the difference in sea surface temperature (SST) between composites of El Niño and La Niña events for five two-month periods during the ENSO cycle: July-August [JA(0)], October-November[ON(0)], January-February [JF(1)], April-May [AM(1)] and July-August [JA(1)], where 0 denotes the year ENSO peaks and 1 the following year. Composites are constructed from ten El Niño (warm) events: 1957, 1965, 1969, 1972, 1976, 1982, 1987, 1991, 1997, and 2002; and ten La Niña (cold) events: 1950, 1954, 1955, 1964, 1970, 1973, 1975, 1988, 1998, and 1999 during 1950-2003.

If we first focus on boreal fall and winter (Plate 1b-c), the ENSO-related signal is strong with positive SSTs ( $>2.0^{\circ}\text{C}$ ) over the eastern half of the tropical Pacific. Beyond the ENSO region, a reduction in the strength of the trade winds and the amount of cloud cover contribute to abnormally warm water in the tropical Atlantic by AM(1) [e.g., Covey and Hastenrath, 1978; Alexander and Scott, 2002; Wu et al., this volume] and over most of the Indian Ocean from ON(0) to AM(1) [e.g., Cadet, 1985; Nicholson, 1997; Klein

et al., 1999]. In the North Pacific, strong cyclonic flow around an anomalously deep Aleutian low during El Niño events cools the central North Pacific and warms the water along the west coast of North America [e.g., Alexander, 1992; Luksch, 1992; Lau and Nath, 1996; Alexander et al., 2002, our Plates 1 and 2 b-d].

El Niño events, however, are already well established by JA(0), when warm water covers the equatorial Pacific (Plate 1a) and positive sea level pressure (SLP) anomalies are located over the eastern hemisphere and negative anomalies over the western hemisphere, characteristic of the negative phase of the Southern Oscillation [e.g. Wang and Picaut, this volume; our Plate 2a]. Unlike JF(1), SST anomalies are negative to the south of Indonesia in JA(0), but like the subsequent winter, they are positive over the western part of the tropical Indian Ocean, leading to an east-west dipole across the basin. The negative anomalies near Indonesia are part of an inter-hemispheric “horseshoe” pattern that extends from the North Pacific to the south-central Pacific. Large amplitude negative SST anomalies have already begun to form in the western North Pacific by JA(0); indeed, one of the largest bridge-related signals occurs during late summer/early fall along  $\sim 40^{\circ}\text{N}$  (Plate 1a and 1b). The composite El Niño minus La Niña SSTs normalized by the monthly standard deviation, shown in Figure 1, indicates the SST anomaly in the western North Pacific region reaches a minimum in September(0) of approximately  $-1\frac{1}{2}$  times the standard deviation (a non-normalized value of  $\sim -1.5^{\circ}\text{C}$ ).

By JA(1) ENSO has all but disappeared with negative SST anomalies along the equator in the eastern Pacific (Plate 1e). Nevertheless, many of the SST anomalies created by the atmospheric bridge, including those in the Indian Ocean, South China Sea and eastern North Pacific, peak in late winter or spring and then persist into early summer, albeit at a smaller amplitude (Plate 1 and Figure 1).

Plate 1 and Figure 1 indicate that the bridge-related SST anomalies vary greatly depending on the region and the phase of the ENSO cycle. Some of these features are fairly well understood, such as the atmospheric teleconnections to the North Pacific Ocean during boreal winter [as reviewed by Alexander et al., 2002] and the bridge to the tropical Atlantic [Wu et al., this volume and references therein]. In this article, we examine two emerging research foci of the atmospheric bridge phenomena. First, we review recent literature concerning the evolution of the atmosphere-ocean system in the tropical Indian and western Pacific Oceans over the course of the ENSO cycle. Second, we perform new analyses of processes that cause large-amplitude SST anomalies in the western North Pacific during the summer of Yr(0). In both regions, air-sea interactions in season

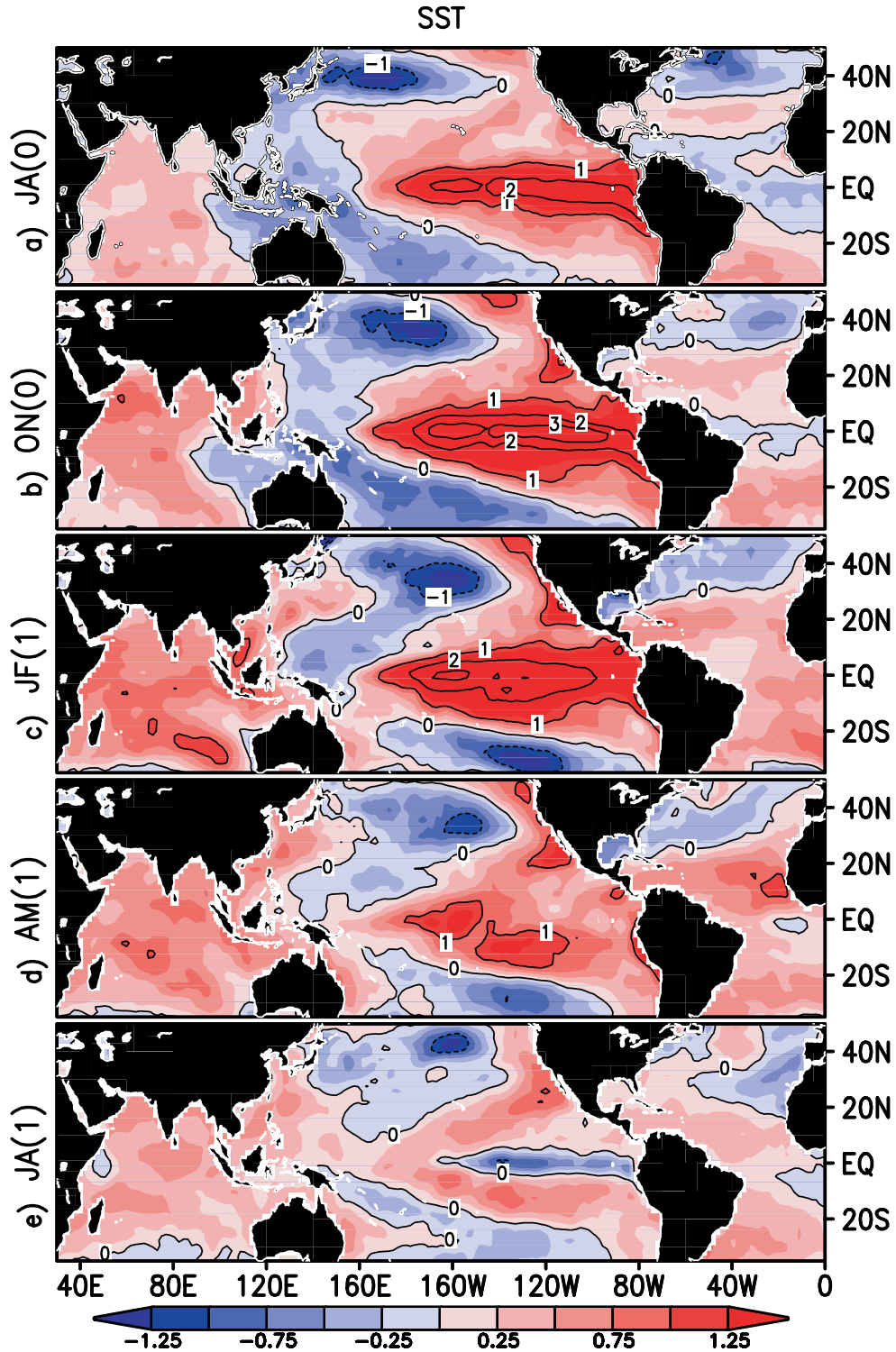


Plate 1. Anomalous SST is constructed by subtracting the composite of 10 El Niño events from the composite of 10 La Niña events in the 1950-2003 period, for a) July-August [JA(0)], b) October-November [ON(0)], c) January-February [JF(1)], d) April-May [AM(1)] and e) July-August [JA(1)], where 0 indicates the ENSO year and 1 the following year. The shading (contour) interval is 0.25 (1.0) °C. The values are obtained from the National Center for Environmental Prediction (NCEP) reanalysis [Kalnay *et al.*, 1996; Klistner *et al.*, 2001].

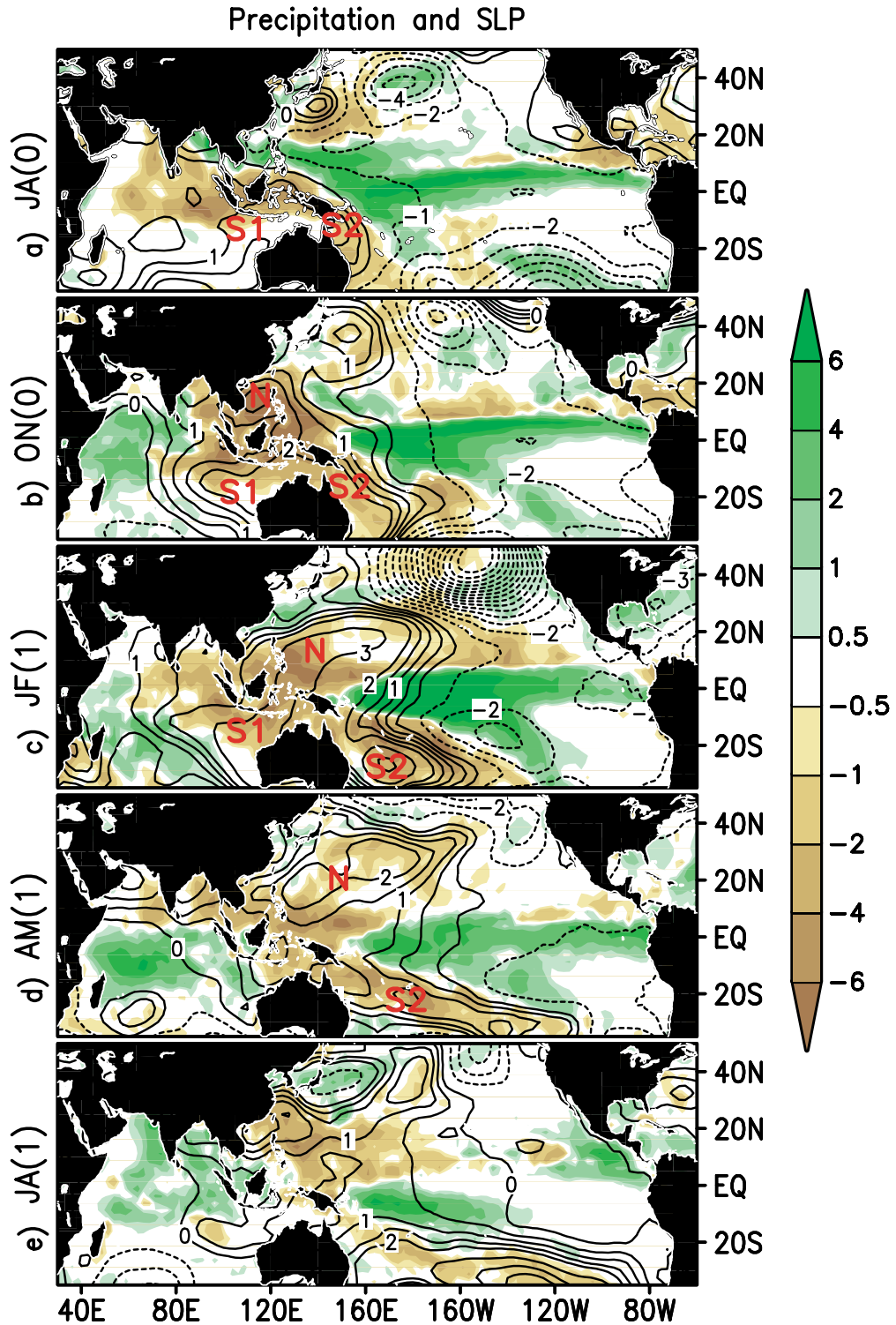


Plate 2. El Niño – La Niña composite sea level pressure (contours, base interval: 1.0 mb; with additional contours for +0.5 and +1.5 mb) and precipitation (shading, see scale at side), based on ENSO events in the 1982-2003 period, for a) JA(0), b) ON(0), c) JF(1), d) AM(1), e) JA(1). The subtropical high pressure anomaly centers are identified by the labels N, S<sub>1</sub> and S<sub>2</sub>. Results for the pressure and precipitation fields are obtained using NCEP/NCAR reanalysis and CMAP data, respectively.

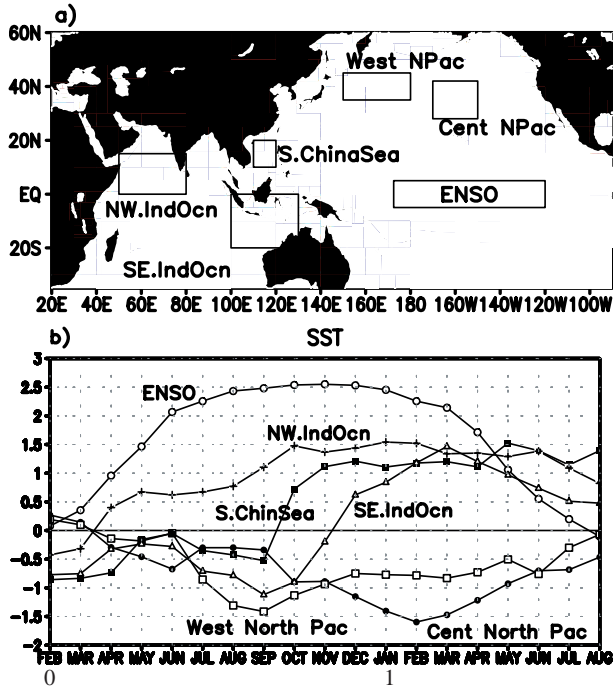


Figure 1. a) Indo-Pacific regions where the ENSO SST signal is strong. b) El Niño – La Niña composite SST from Feb(0) to Aug(1) normalized by the SST standard deviation in each calendar month for the regions shown in (a). The regions are located in the central equatorial Pacific (ENSO; 5°S-5°N, 172°E-120°W), Western North Pacific (WNP; 35°N-45°N, 150°E-180°), Central North Pacific (28°N-42°N, 170°W-150°W), northwest Indian Ocean (0°-15°N, 50°E-80°E), southeast Indian Ocean (0°-20°S, 100°E-130°E), and the South China Sea (10°N-20°N, 110°E-120°E). While the magnitude of the ENSO anomalies is much larger in winter than in summer, the weak summer variability results in nearly uniform normalized ENSO SST anomalies from August(0) to January(1).

other than boreal winter have the potential to feedback on the broader climate system.

## 2. INDIAN AND SUBTROPICAL WESTERN PACIFIC OCEANS

To delineate the role of the atmosphere in communicating ENSO's effect on the Indo-Pacific sector, the composite procedure adopted in Plate 1 has been applied to selected meteorological fields. The results for various stages of the ENSO life cycle are displayed in Figure 2 for surface wind vectors and Plate 2 for SLP (contours) and precipitation (shading). The patterns in Figure 2 are based on NCEP reanalysis data for the 10 warm and 10 cold events. The SLP and precipitation composites in Plate 2 are computed with NCEP reanalysis and Climate Prediction Center (CPC) Merged Analyses of Precipitation [CMAP, *Xie and Arkin,*

1997] data, respectively, for the ENSO events occurring in 1982-2002. We use the CMAP data as they are considered more reliable than the precipitation estimates from NCEP reanalysis. Similar ENSO-related anomalies were found using precipitation and SLP for the composite of the 10 warm – 10 cold ENSO events from reanalysis (not shown).

The tropical atmospheric response to ENSO, the first element in the atmospheric bridge, is well established even during the very early stages of the ENSO cycle: surface convergence and precipitation are enhanced across the tropical Pacific from the South American coast to 160°E between 0°-10°N in JA(0) (Figure 2a and Plate 2a). These anomalies increase in magnitude and meridional extent through JF(1), then weaken by AM(1) and dissipate by JA(1). Changes in diabatic heating associated with the precipitation anomalies over the equatorial Pacific drive atmospheric circulation changes connecting the ENSO region to the tropical portion (25°N-25°S) of the Indian and West Pacific Oceans, as discussed in the following subsections.

### 2.1. Indian Ocean

The most notable development in the SLP pattern during the JA(0)-JF(1) period is the emergence of a high anomaly center (denoted as S1 in Plate 2a-c) off the northwestern Australian coast. Stationary wave modeling [e.g., *Wang et al.* 2000, 2003; *Lau et al.*, 2004a] indicates that this feature is a Rossby wave response to the reduced latent heating over the equatorial western Pacific and Indonesia (mainly due to the reduction in precipitation seen in Plate 2a-c), where the subsiding branch of the anomalous Walker Circulation resides during El Niño events. In the northern summer and early autumn, the climatological flow is directed northwestward over much of the Indian Ocean (IO) basin south of the Equator, and eastward just north of the Equator [e.g., Figure 1 in *Schott and McCreary*, 2001]. Hence the anomalous circulation in the vicinity of S1 from June to October (Figure 2a-b) is associated with above-normal wind speeds (not shown) over the waters off the Sumatra/Java coasts, which enhance heat loss from the ocean as well as coastal upwelling [e.g. *Murtugudde et al.*, 2000; *Iizuka and Matsura*, 2000; *Li et al.*, 2002; *Lau and Nath*, 2004]. These processes contribute to the occurrence of cold SST anomalies forming off the southern coasts of Java and Sumatra, and the northwestern coast of Australia (Plate 1a-b and Figure 1). Conversely, the below-normal wind speeds on the western flank of S1 as well as over the central equatorial IO during austral spring are accompanied by decreases in the oceanic heat loss and SST warming. This east-west SST contrast peaks in boreal fall, as indicated by the difference between the composite SST anomalies in the northwest and southeast IO regions (Plate 1b and Figure 1).

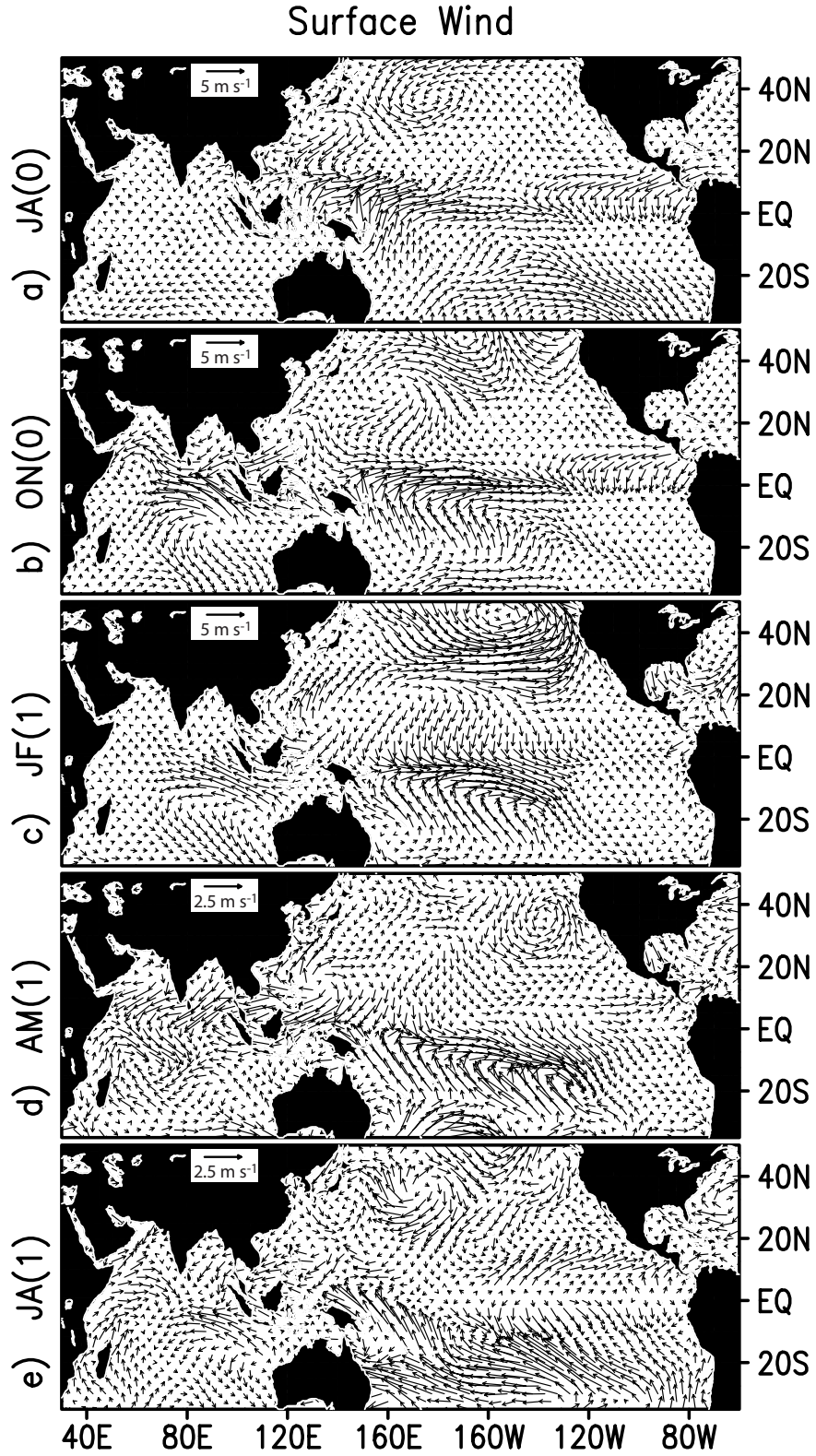


Figure 2. El Niño – La Niña composite surface vector winds (scale vector upper left corner of each panel), for (a) JA(0), (b) ON(0), (c) JF(1), (d) AM(1), and (e) JA(1). Values are from NCEP/NCAR reanalysis data for the period 1950-2003. Note that scale vector in (a)-(c) differs from that in (d)-(e).

The overall SST, wind circulation, SLP and precipitation patterns in Plate 1b, Figure 2b and Plate 2b bear a strong resemblance to those associated with a prominent “dipole mode” of atmosphere-ocean variability in the IO basin, as described by *Saji et al.* [1999] and *Webster et al.* [1999]. The appearance of this characteristic mode in the ENSO-based composites presented here suggests that ENSO events could play a considerable role in the zonally asymmetric SST anomaly pattern occurring in IO during the boreal summer and autumn. The influence of ENSO on atmosphere-ocean variability in the IO sector have been emphasized in the observational analysis of *Allan et al.* [2001] and *Hendon* [2003], and the modeling studies of *Lau and Nath* [2004] and *Shinoda et al.* [2004]. There exists, however, empirical and model evidence for the occurrence of anomalous events with an east-west SST contrast when ENSO is absent in the tropical Pacific [*Saji and Yamagata*, 2003; *Lau and Nath*, 2004; *Yamagata et al.*, this volume].

With the approach of the summer monsoon season over northern Australia, the climatological flow above the waters south of Sumatra/Java switches from easterly to westerly by November and remains westerly through February [e.g., *Shinoda et al.*, 2004]. The southeasterly wind anomaly occurring at this time and location (Figure 2b-c) is therefore directed against the time mean circulation. The resulting decrease of the local wind speed reduces both oceanic heat loss and upwelling, reversing the cold SST anomaly in the eastern IO south of the Equator [*Li et al.*, 2003; *Lau and Nath*, 2004]. The northwesterly wind anomalies situated to the west of S1, suppress the wind speed over the south central IO through JF(1), and thus enhance the warm SST anomaly in that region. The contributions of surface latent heat fluxes to SST changes in various parts of IO during ENSO have previously been emphasized in the observational analyses of *Yu and Rienecker* [1999] and modeling studies of *Behera et al.* [2000] and *Venzke et al.* [2000]. Rossby waves generated by anomalous winds in the southwestern IO may also lead to basin-wide warming by JF(0) [*Chambers et al.*, 1999].

During ON(0), below normal precipitation prevails over the cold SST anomaly in the eastern tropical IO, whereas wet conditions occur over the warm anomaly off the eastern African coast (Plates 1b and 2b). The dryness over the eastern IO is accompanied by reduced cloud cover and enhanced shortwave heating of the ocean surface, resulting in the dissipation of the cold SST anomaly in that region [*Klein et al.*, 1999; *Li et al.*, 2002; *Shinoda et al.*, 2004].

In the boreal winter and spring of Yr(1), a broad positive precipitation anomaly extends across the IO south of the Equator (Plate 2c-d), where above-normal SST prevails (Plate 1c-d). During the AM(1) period (Figure 2d), both the orientation of the anomalous cross-equatorial flow from the northern IO towards this rainbelt, and the development of cyclonic circulation in the surface wind field over 0°-30°S,

60°E-90°E, situated to the west of the precipitation maximum, suggest that these atmospheric circulation features are the response to the underlying SST anomaly pattern and the associated condensational heating aloft [e.g., see discussions in *Hoskins and Karoly*, 1981; *Xie et al.*, 2002]. Hence the SST changes in the IO basin, which were partially driven by the atmospheric bridge mechanism in the previous seasons, influence the atmospheric circulation in AM(1).

## 2.2. Subtropical Western Pacific

The atmospheric pattern over the South China and Philippine Seas during the summer of Yr(0) is characterized by cyclonic wind anomalies (westward winds near 20°N and eastward winds near 10°N in Figure 2a) and more intense rainfall (Plate 2a). These features are indicative of a more eastward extension of the summer monsoon trough to the subtropical western North Pacific, and are probably associated with the Rossby wave response to the latent heat release accompanying the enhanced precipitation near the dateline during El Niño events (Plate 2a). The attendant increase in surface wind speed is conducive to below normal SST along the Chinese coast and the Philippine Sea.

High pressure anomalies, denoted by S2 and N, appear over the northeastern Australian coast and the South China Sea in JA(0) and ON(0), respectively (Plates 2a and 2b), these features migrate eastward in the following months (Plates 2c-2d). Results from mechanistic models [*Wang et al.*, 2003; *Lau et al.*, 2004a] indicate that, in analogy with the forcing of S1, the high centers in the western Pacific are also Rossby-wave responses to the below-normal condensational heating in the Indonesian sector. Over the subtropical northwestern Pacific, the time mean circulation in the northern autumn and winter seasons is dominated by the northeasterly monsoon off the eastern Asian seaboard [e.g., *Lau and Nath*, 2000]. The southwesterly anomalous flow on the northwestern flank of the anticyclonic center N impedes the strength of the climatological monsoon (Figures 2b and 2c), thereby warming the waters in the South China and East China Seas in ON(0) and JF(1) [Plate 1, also see *Wang et al.*, 2000 and *Lau et al.*, 2004a]. On the other hand, the northwesterly anomalous circulation located southeast of N in ON(0) is coincident with increased wind speeds and SST cooling; as discussed in greater detail by *Wang et al.* [2000]. An analogous set of local relationships between the mean circulation and the anomalies in the wind and SST fields is discernible among the features associated with S2. The superposition of the anomalous counterclockwise circulation on the climatological southeasterly flow in that region results in below normal wind speeds and warm SSTs off the southeast Australian coast.

The anomalous precipitation pattern over the northwestern subtropical Pacific in ON(0)-JF(1) (Plate 2b-2c) is characterized by dryness in the vicinity of N. Due to weakening of the dry winter monsoon over East Asia [Wang *et al.*, 2000], above-normal precipitation amounts are seen over the East China Sea.

In AM(1), the anomalous anticyclonic circulation around the high pressure anomaly N remains clearly evident (Figure 2d and Plate 2d), with the center of N extending slightly farther to the northeast relative to its locations in the previous autumn and winter. The observational and model evidence presented by Wang and Zhang [2002], Wang *et al.* [2003] and Lau *et al.* [2004a] imply that local air-sea thermodynamic feedbacks play a crucial role in the sustenance and eastward migration of N. Anomalous high pressure and dry conditions are still evident in JA(1) over much of the subtropical western North Pacific from the Chinese coast to  $\sim 170^\circ\text{E}$  (Plate 2e).

2.3. Discussion

Comparison of the composite patterns over both the Indian and the subtropical western Pacific Oceans for JA(0) and JA(1) reveals interesting differences between anomalies occurring during northern summer in the two consecutive years. Of particular note is the transition to the east of the Phillipines from cyclonic circulation and enhanced rainfall in Yr(0) to anticyclonic circulation and reduced rainfall in Yr(1). The switch in polarity (from cold to warm) of the SST anomaly in the eastern portion of the IO basin is related to a local reduction in precipitation in Yr(0) and enhanced precipitation in Yr(1). The tendency for the anomalies in the above locations to change their polarities from one year to the next is one facet of the Tropospheric Biennial Oscillation (TBO) of Asian-Australian monsoon system [see the review by Meehl, 1997]. The results and discussions presented in this section suggest that the seasonal dependence of local air-sea coupling as well as responses of the atmosphere-ocean system in the Indo-Pacific to remote ENSO forcing is an important factor for understanding the origin of some of the phenomena associated with the TBO.

Tropical SST anomalies associated with the atmospheric bridge influence the large-scale atmospheric circulation well after ENSO has peaked. The persistence of tropical SST anomalies outside the equatorial east Pacific contributes to the delayed atmospheric response to ENSO: e.g. the zonal mean 200 mb height anomalies between  $30^\circ\text{N}$ - $30^\circ\text{S}$  are three times stronger in the summer of Yr(1) than the summer of Yr(0), despite stronger SST anomalies in the Niño region in Yr (0) [Kumar and Hoerling, 2003]. ENSO-induced SST anomalies in the Indo-Western Pacific sector also exert a strong influence on the Asian monsoon system, where the accompanying redistribution of

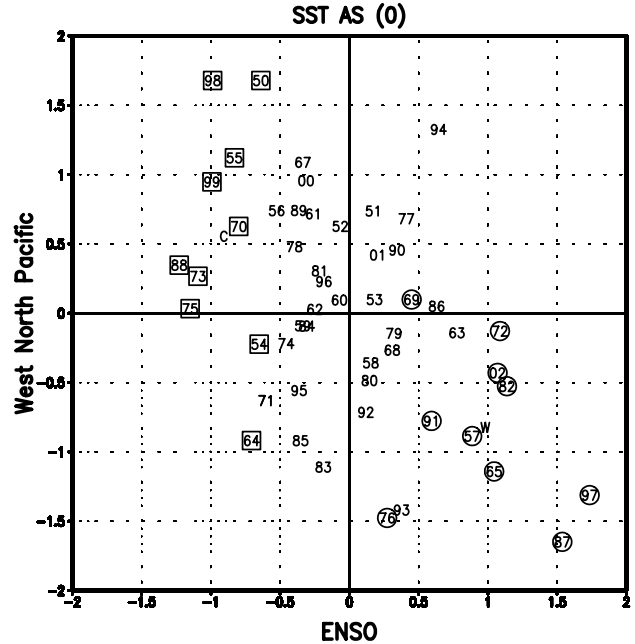


Figure 3. Scatter diagram of the SST anomalies ( $^\circ\text{C}$ ) in AS(0) relative to the 1950-2003 mean, in the ENSO and WNP regions (domains shown in Figure 1a). The values of the ten individual El Niño (La Niña) events are enclosed in circles (squares) and the composite average is denoted by a W (C).

condensational heat sources and sinks leads to marked changes in the strength and position of the Asian jet stream [Lau *et al.*, 2004b]. The effects of these atmospheric perturbations are extended eastward across the extratropical North Pacific through dynamical interactions between the quasi-stationary flow and synoptic-scale transient eddies, such as those described in Section 3.1. Lau *et al.* [2004b] further noted that this chain of processes contributes to summertime anomalies in the zonally averaged circulation in midlatitudes, as well as the regional climate over North America (e.g., occurrence of droughts and prolonged heat waves).

3. NORTH PACIFIC IN SUMMER OF YR(0)

3.1. SST

In overviews of the SST and atmospheric surface changes that typically occur during ENSO periods, Harrison and Larkin [1998], Wang [2002], and Park and Leovy [2004] found that cold SST anomalies are centered along  $\sim 40^\circ\text{N}$  in the western half of the North Pacific in summer and fall of Yr(0). These negative summertime SST anomalies are also readily apparent from the leading mode of SST variability based on rotated empirical orthogonal functions (EOFs) of Pacific SST variability in all calendar months [Barlow *et al.*, 2001]. We examine the association between SST

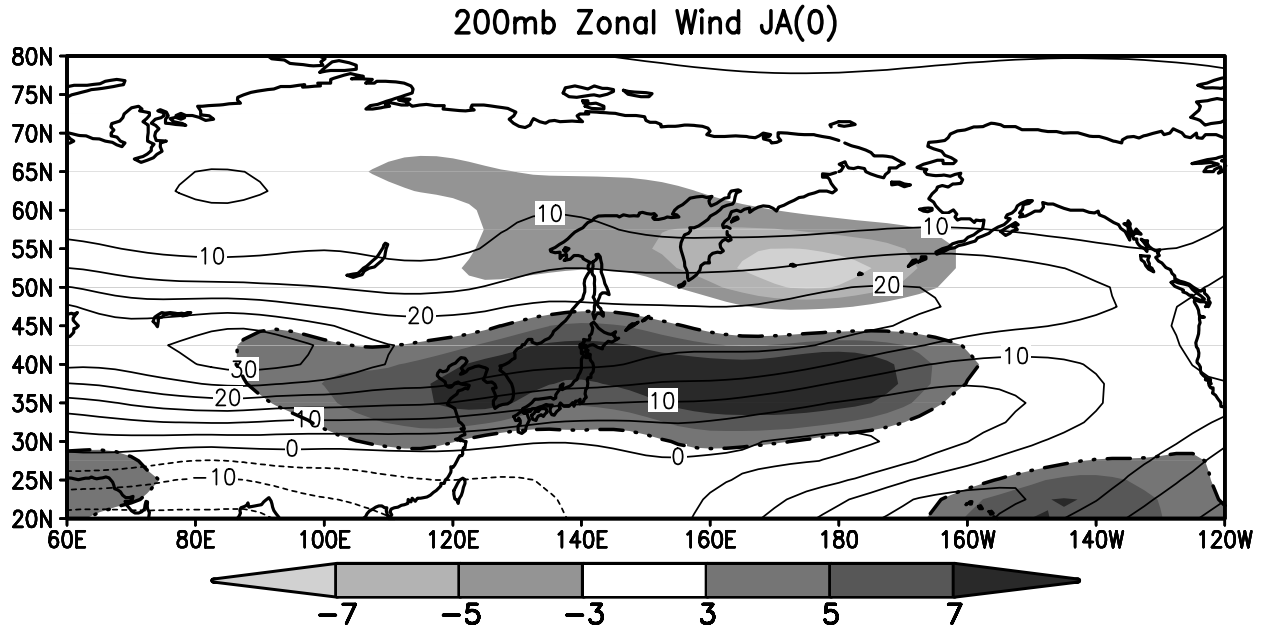


Figure 4. The climatological mean zonal wind (contours, interval:  $5 \text{ m s}^{-1}$ ) during July-August and composite El Niño – La Niña zonal wind (shading, scale at bottom; regions  $> 3 \text{ m s}^{-1}$  enclosed by a dot-dash line) during JA(0) from NCEP reanalysis for ENSO events between 1950-2003.

anomalies in the central-eastern equatorial Pacific and the western North Pacific (the ENSO and WNP regions shown in Figure 1a) via a scatter diagram of the departures of SSTs in Aug-Sep in the years 1950-2002 from their long-term mean over this period in Figure 3. The relationship between SSTs in the ENSO and WNP regions is quite strong: *i*) the correlation between the two regions over all 52 summers is  $-0.49$  (significant at the 99% level), *ii*) the composite difference between the warm and cold phases of ENSO is  $\sim -1.45^\circ\text{C}$  in the northwest Pacific (significant at the 99% level), and *iii*) the SST anomalies in the northwest Pacific region are negative in 9 of 10 El Niño events and positive in 8 of 10 La Niña events. While the negative SST anomalies in the northwest Pacific region are somewhat larger in amplitude and exhibit less scatter than the positive anomalies, it is unclear whether this represents a non-linear difference in the remote oceanic response to the warm and cold phases of ENSO, or is merely due to the limited number of samples. The atmospheric and oceanic processes that contribute to the formation of North Pacific SST anomalies during the summer of ENSO events are examined in the following subsections.

### 3.2. Atmospheric Circulation

The atmospheric response to ENSO is not confined to the tropics, and teleconnections to the Pacific North American sector occur during much of the ENSO cycle. The dynamical link between the tropics and extratropics [as re

viewed by *Trenberth et al.*, 1998] are complex involving the excitation of Rossby waves by tropical convection, the propagation of these waves to midlatitudes and their subsequent interaction with asymmetries in the zonal mean flow and with midlatitude storm tracks.

While most studies of the atmospheric processes linking the tropics and extratropics were based on conditions during boreal winter, the few investigations that considered other seasons found that there could be strong teleconnections in summer as well. The initial analyses of ENSO-related teleconnections in summer were motivated by the severe drought in the central United States during the summer of 1988 [*Trenberth et al.*, 1988; *Mo et al.*, 1991; *Palmer and Brankovic*, 1989; *Trenberth and Branstator*, 1992]. Several factors may enable ENSO to influence the extratropical circulation in summer despite the broad latitudinal extent of the mean easterlies in the tropical troposphere that act as a barrier to Rossby wave propagation. These include SST and precipitation (heating) anomalies in the subtropics (e.g. see Plates 1a and 2a), Rossby waves created by local divergent circulations, and longitudinal and/or height variations in the mean zonal wind that allow Rossby waves to propagate to the midlatitudes [*Nitta* 1986, 1987; *Lau and Peng*, 1992; *Chen and Yen*, 1993; *Trenberth and Branstator*, 1992; *Grimm and Silva Dias*, 1995; *Newman and Sardeshmukh*, 1998]. Heating anomalies associated with the Asian monsoon [*Lau and Weng*, 2002] and ENSO induced changes in extratropical transients [*Kok and Opsteegh*,

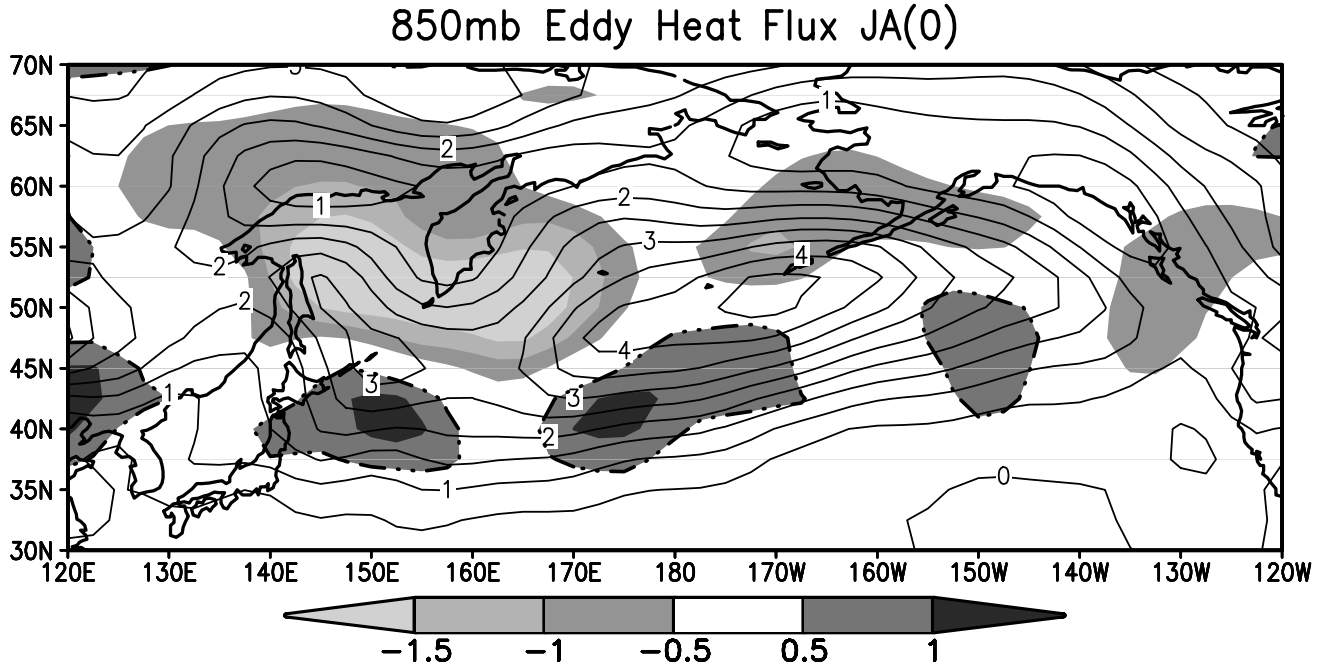


Figure 5. The climatological mean eddy meridional heat transport ( $\overline{v'T'}$ ) (contours, interval:  $0.5^\circ\text{Cm s}^{-1}$ ) during July-August and El Niño – La Niña composite  $\overline{v'T'}$  (shading, scale at bottom; regions  $> 0.5^\circ\text{Cm s}^{-1}$  enclosed by a dot-dash line) at 850 mb during JA(0). The prime denotes the departure from the monthly mean that is then band pass (2-8 day) filtered and an overbar denotes the time average over JA. The values were obtained from NCEP reanalysis for ENSO events between 1950-2003.

1985] may also contribute to the height anomalies over the North Pacific in summer.

Here we examine the circulation and storm track anomalies over the North Pacific in summer of Yr(0). During JA (0), positive (negative) zonal wind anomalies form to the south (north) of the climatological mean jet axis at  $\sim 40^\circ\text{N}$  over eastern Asia and the western half of the North Pacific (Figure 4). The anomalies are approximately 25-50% of the mean winds, representing a substantial southward shift in the Asian-Pacific jet. (The mean jet is about  $\frac{1}{2}$  as strong and  $\sim 15^\circ$  farther north in summer than in midwinter). The El Niño-La Niña composite difference in the Pacific storm track, as measured by the band pass (2-8 day) filtered meridional heat transport at 850 mb ( $\overline{v'T'}$ ), is shown in Figure 5. Like the seasonal mean changes in the jet stream, the anomalous eddy heat transport also indicates a southward shift in the storm track over much of the North Pacific.

Following previous studies of the relationship between the low frequency circulation anomalies and synoptic eddies in winter [e.g. Lau and Holopainen, 1984; Lau, 1988], we compare the anomalous geopotential height ( $z$ ) and eddy induced height tendency ( $z_t$ ) in the upper troposphere in summer; presented here as the difference between El Niño and La Niña composites of both quantities at 200 mb averaged over JA (0). The synoptic forcing is derived from the contribution of the band pass filtered eddy

vorticity flux divergence ( $\nabla \cdot \overline{v'\zeta'}$ ) to the vorticity tendency at the 200 mb level, and then converting the vorticity tendency to height tendency by assuming geostrophy, e.g.

$$z_t = \frac{f}{g} \nabla^{-2} (\nabla \cdot \overline{v'\zeta'}), \quad (1)$$

where  $f$  the Coriolis parameter,  $g$  the acceleration due to gravity,  $\overline{v}$  the horizontal wind vector,  $\zeta$  the vorticity. The changes in the jet (Figure 4) are consistent with geostrophic flow around a negative  $z$  anomaly that extends from central Asia to the central Pacific along  $45^\circ\text{N}$  and positive anomaly over eastern Siberia (contours in Figure 6); this pair of anomalies resembles the Pacific-Japan pattern [Nitta, 1987] and the North Pacific teleconnection pattern (Barnston and Livezey, 1987). The synoptic forcing (shading) is large ( $z_t > 5 \text{ md}^{-1}$ ) and nearly collocated with the height anomalies, suggesting that the synoptic eddies strongly contribute to the seasonal circulation anomalies. The  $z_t$  anomalies, however, are displaced slightly to the west of the  $z$  anomalies. The time scale of the eddy forcing,  $z/z_t$ , is  $\sim 10$  days, indicating that horizontal eddy forcing in the upper troposphere is rapid enough to generate the observed summer height anomalies. Results from previous studies [e.g. Ting and Lau, 1993] indicate that other processes, such as eddy heat flux forcing, diffusion, etc., somewhat compensate the height changes initiated by  $z_t$ .

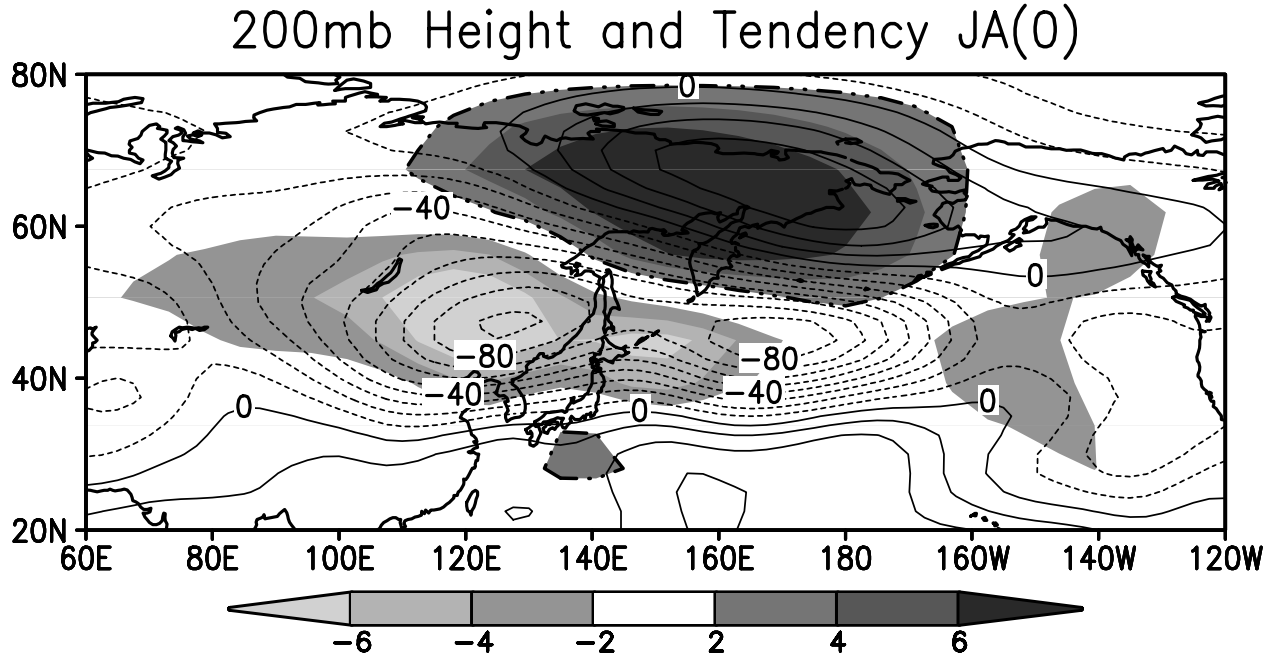


Figure 6. The El Niño – La Niña composite geopotential height (contours, interval: 10 m) and the eddy induced height tendency (shading, scale at bottom; regions  $> 2 \text{ m d}^{-1}$  enclosed by a dot-dash line) at 200 mb during JA (0). The height tendency, is given by equation (1). The values were obtained from NCEP reanalysis for ENSO events between 1950-2003.

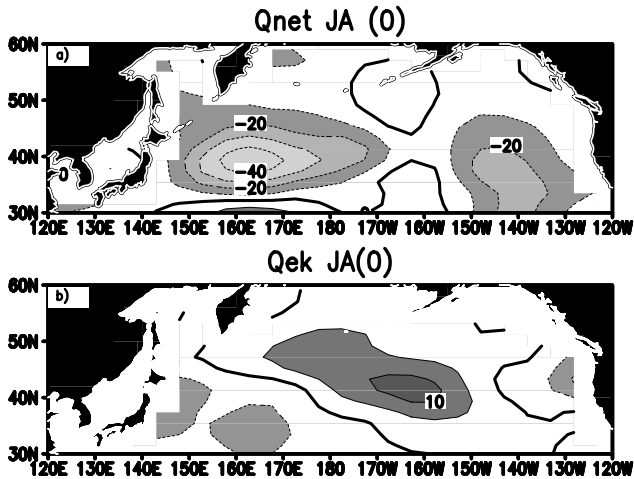


Figure 7. Composite El Niño – La Niña a) net heat flux into the ocean ( $Q_{net}$ ) and b) Ekman heat transport in flux form ( $Q_{ek}$ ) in JA(0) during ENSO events from 1983-2000. In (a) the contour interval is  $10 \text{ W m}^{-2}$  and shading transitions occur at  $-10$ ,  $-20$  and  $-40 \text{ W m}^{-2}$ , in (b) the shading and contour intervals are both  $5 \text{ W m}^{-2}$ . The radiative fluxes used in  $Q_{net}$  are derived from satellite data [Zhang and Rossow; 2003], while the sensible and latent fluxes used to compute  $Q_{net}$  are derived from NCEP reanalysis. Reanalysis is also used to compute  $Q_{ek}$  in equation (2).

In addition to interacting with the large-scale circulation patterns, synoptic eddies also influence clouds. Low clouds associated with traveling cyclones are prevalent over the North Pacific during summer, where the cloud fraction

exceeds 60% north of  $\sim 40^\circ\text{N}$  and rapidly decreases towards the subtropics [Weaver and Ramanathan, 1996; Norris and Leovy, 1994]. The leading interannual pattern of stratus cloud variability in summer is located where the gradient in the mean cloud amount is strongest, i.e. the central and west Pacific between about  $30^\circ\text{N}$ - $45^\circ\text{N}$ , and is associated with meridional displacements in the storm track and the underlying SST [Norris, 2000]. Recently, Park and Leovy [2004] found that much of the interannual fluctuations in the storm track, cloud amount and SST over the North Pacific in summer are associated with ENSO variability. The changes in the storm track and cloud amount (not shown) are consistent with enhanced precipitation and reduced SLP in the vicinity of  $40^\circ\text{N}$ ,  $170^\circ\text{W}$  during El Niño relative to La Niña events (Plate 2a). The passage of more and/or stronger synoptic disturbances cools the ocean by increasing cloudiness, which reduces the solar radiation reaching the surface.

### 3.3. Surface fluxes

The ENSO-driven atmospheric circulation changes over the North Pacific influence the SST directly via the net heat flux and indirectly via momentum and fresh water fluxes that subsequently affect ocean currents and turbulent mixing. Here we consider two key factors that influence SST anomalies on interannual time scales: the net surface heat flux ( $Q_{net}$ ) and the Ekman heat transport in flux form:

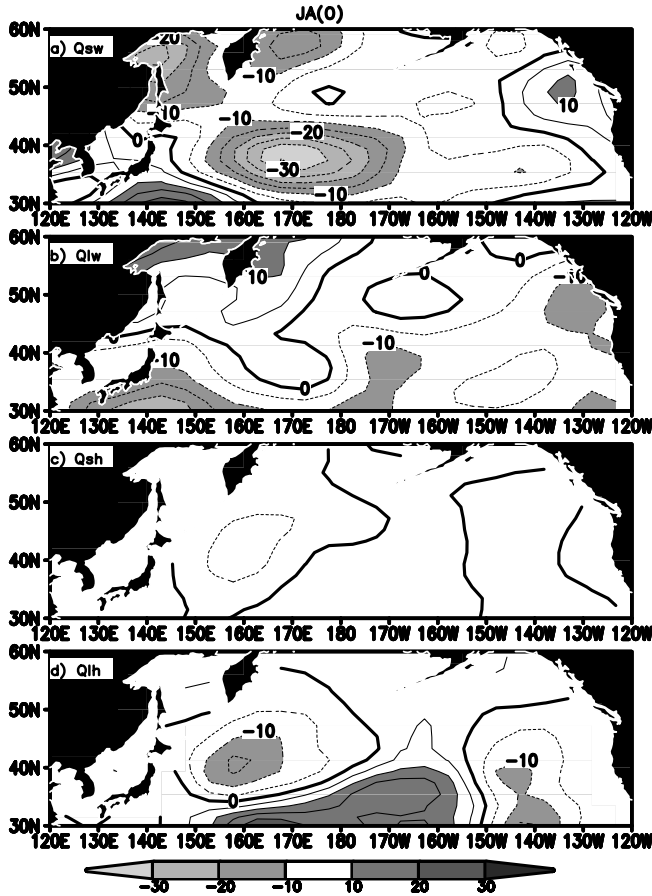


Figure 8. Composite El Niño - La Niña surface a) shortwave ( $Q_{sw}$ ), b) longwave ( $Q_{lw}$ ), c) sensible ( $Q_{sh}$ ) and d) latent ( $Q_{lh}$ ), fluxes in JA(0) during ENSO events from 1983-2000. The contour interval is  $5 \text{ W m}^{-2}$ . Shading interval indicated by scale at bottom.

$$Q_{ek} = \frac{c}{f} \left[ -\tau_y \frac{\partial}{\partial x} SST + \tau_x \frac{\partial}{\partial y} SST \right], \quad (2)$$

where  $c$  is the specific heat of seawater, parameter,  $\tau_x$  and  $\tau_y$  are the zonal and meridional components of the surface wind stress.

The net surface heat flux depends on four components: the short wave ( $Q_{sw}$ ) and long wave ( $Q_{lw}$ ) radiation, and the sensible ( $Q_{sh}$ ) and latent ( $Q_{lh}$ ) heat flux. The  $Q_{sh}$  and  $Q_{lh}$  values used here are from NCEP reanalysis. However, the  $Q_{sw}$  values from reanalysis have been shown to have large errors [e.g. *Scott and Alexander, 1999*], so we use the  $Q_{sw}$  and  $Q_{lw}$  estimates derived from the International Satellite Cloud Climatology Project [ISCCP; *Zhang et al., 1995; Rossow and Zhang, 1995, Zhang and Rossow, 2004*]. The flux composites presented in Figures 7 and 8 are based on ENSO events from 1983-2000, the period when radiative fluxes derived from ISCCP data are available. The El Niño - La Niña composites of  $Q_{net}$  and  $Q_{ek}$  for JA(0) are displayed in Figure 7, when the SST decreases rapidly in

the western North Pacific (WNP) region (Plate 1 and Figure 1). The WNP region is strongly cooled by  $Q_{net}$ , as indicated by negative values ( $< -40 \text{ W m}^{-2}$ ) between approximately  $150^\circ\text{E}-180^\circ$ ,  $35^\circ\text{N}-42^\circ\text{N}$ . The  $Q_{ek}$  anomalies, while much smaller, also cool the ocean between  $30^\circ\text{N}-45^\circ\text{N}$  from Japan to the dateline (Figure 7b). This anomalous cooling is located about  $\sim 5^\circ$  further south in the ENSO composite based on all events between 1950-2003 (not shown), which is consistent with the anomalous westerly winds between approximately  $25^\circ\text{N}-38^\circ\text{N}$  (Figure 2a) that enhance the southward transport of cold water in the western North Pacific.

The ENSO composite anomalies for each of the four flux components are presented in Figure 8. Unlike winter, when  $Q_{sw}$  anomalies are negligible, during JA(0) the ENSO-related shortwave radiation anomalies have the largest magnitude of the four components.  $Q_{sw}$  cools the ocean in the vicinity of  $35^\circ\text{N}$ ,  $170^\circ\text{E}$ , consistent with the ENSO-induced increase in low-level clouds [*Park and Leovy, 2004*] and precipitation over the northwest Pacific (Plate 2a). The  $Q_{lw}$  and  $Q_{sw}$  radiation anomalies tend to be of opposite sign but the former are of modest amplitude. The anomalous  $Q_{lh}$  and to a lesser degree  $Q_{sh}$  also cool the WNP region, although they are located slightly west of the main  $Q_{sw}$  anomaly center.

### 3.4. Mixed layer depth

The surface layer of the ocean is generally well mixed, and as a result, the temperature and salinity is nearly uniform over this layer. In winter, the climatological MLD over the North Pacific ranges from approximately 100 m along the west coast of the United States to 250 m to the east of Japan [e.g. *White, 1995; Monterey and Levitus, 1997*], and the mixed layer depth (MLD) anomalies associated with El Niño events exceed 15 m in the central North Pacific [*Alexander et al., 2002*]. As the wind stirring and negative buoyancy forcing (surface cooling) decrease from winter to spring, the climatological mixed layer shoals rapidly and is on the order of 15-20 m during the summer over the North Pacific Ocean [*Monterey and Levitus, 1997*, our Figure 9]. During El Niño events, the southward shift in the storm track, and the associated changes in surface winds and heat flux, act to deepen (shoal) the mixed layer from  $35^\circ\text{N}-46^\circ\text{N}$  ( $48^\circ\text{N}-55^\circ\text{N}$ ) across much of the Pacific in JA(0) (Figure 9). While the amplitude of the ENSO-related mixed layer depth anomalies is smaller in summer compared to winter, the MLD is approximately 10-30% greater during El Niño than La Niña events during late summer/early fall in the WNP region and 30-50% in a sub-region centered slightly to the east (Figures 9 and 10), comparable to or even larger than the fractional change in MLD during winter.

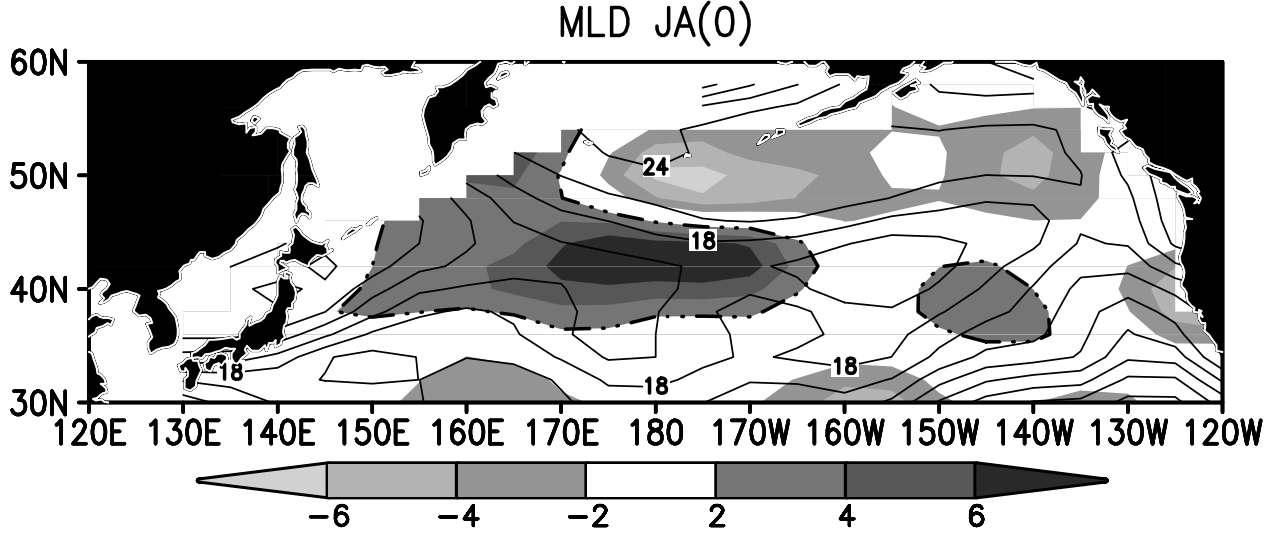


Figure 9. The climatological mean mixed layer depth (contours: interval 3 m) during Jul-Aug and composite El Niño – La Niña mixed layer depth (shading: scale at bottom; values  $> 2$  m are enclosed by a dot-dash line) during JA(0). The mean and ENSO MLD values, derived from ocean temperature observations as described by *White* [1995] for the period 1955-2001, have been spatially smoothed using a 9-point filter.

### 3.5. SST Tendency

The vertical distribution of the temperature anomalies in the WNP region as a function of the ENSO cycle is shown in Figure 10a, based on output from the NCEP Ocean assimilation system [Derber and Rosati, 1989; Ji. et al., 1995] during 1982-2003. Clearly, the ENSO-induced temperature anomalies in the WNP region are confined to the mixed layer through the first year of the ENSO cycle. The mixed layer temperature is influenced by the surface heat flux, Ekman and geostrophic transports, penetrating solar radiation, and entrainment of water through the base of the mixed layer [e.g. *Frankignoul*, 1985]. For well-mixed surface layers the SST tendency is determined by the fluxes into the mixed layer integrated over the MLD. As a result, the ENSO-induced SST response to the same forcing is much greater in AS(0) compared to JF(1), since the mean MLD in the northwest Pacific is approximately an order of magnitude smaller during summer compared to winter.

The ENSO-related ocean temperature anomalies are likely driven by local processes, since they develop rapidly and are confined to the thin surface layer; advection by geostrophic currents is a relatively slow process and operates over depths that are much greater than the MLD. We examine the extent to which the North Pacific SST anomalies are driven by surface fluxes and Ekman transport by comparing the inferred SST tendency, given by

$$Q_t = [Q_{net} + Q_{ek}] / \rho c MLD, \quad (3)$$

where  $\rho$  is the density of seawater) to the actual SST tendency ( $SST_t$ ).  $Q_t$  is computed using three data sets:  $Q_{lh}$  and  $Q_{sh}$  are from NCEP reanalysis [Kistler et al., 2001],  $Q_{sw}$  and  $Q_{lw}$  are derived from ISCCP data [Zhang and Rossow, 2003] and the MLD is based on ocean temperature profiles [White, 1995]. The composite ENSO anomalies of  $Q_t$  (contours) and  $SST_t$  (shaded) are shown over the North Pacific during JA(0) in Plate 3. Both  $Q_t$  and  $SST_t$  indicate rapid cooling in the western North Pacific (32°N-45°N, 150°E-180°), with smaller areas of anomalous warming and cooling in the central and eastern parts of the basin, respectively. In the WNP, the deeper MLD during El Niño compared to La Niña events (Figures 9 and 10) acts to amplify the anomalous SST tendency in the latter, since the forcing is integrated over a thinner layer. During JA(0) the anomalous  $Q_t$  and  $SST_t$  are  $-2.4^\circ\text{C}$  and  $-2.2^\circ\text{C}$ , respectively, when averaged over the northwest Pacific region. The agreement between the observed forcing and the SST response is surprisingly good, given the errors inherent in observations (especially considering that three independent data sources were used to compute  $Q_t$ ) and that several forcing terms were neglected in equation (3).

### 3.6. Discussion

The atmospheric teleconnections associated with ENSO appear to strongly influence North Pacific SST anomalies in the summer of Yr(0), but do these anomalies have a broader impact on climate variability; i.e. does the summertime bridge influence the basin-wide SST characteristics and to what extent does the ENSO-generated SST changes feedback on the atmosphere?

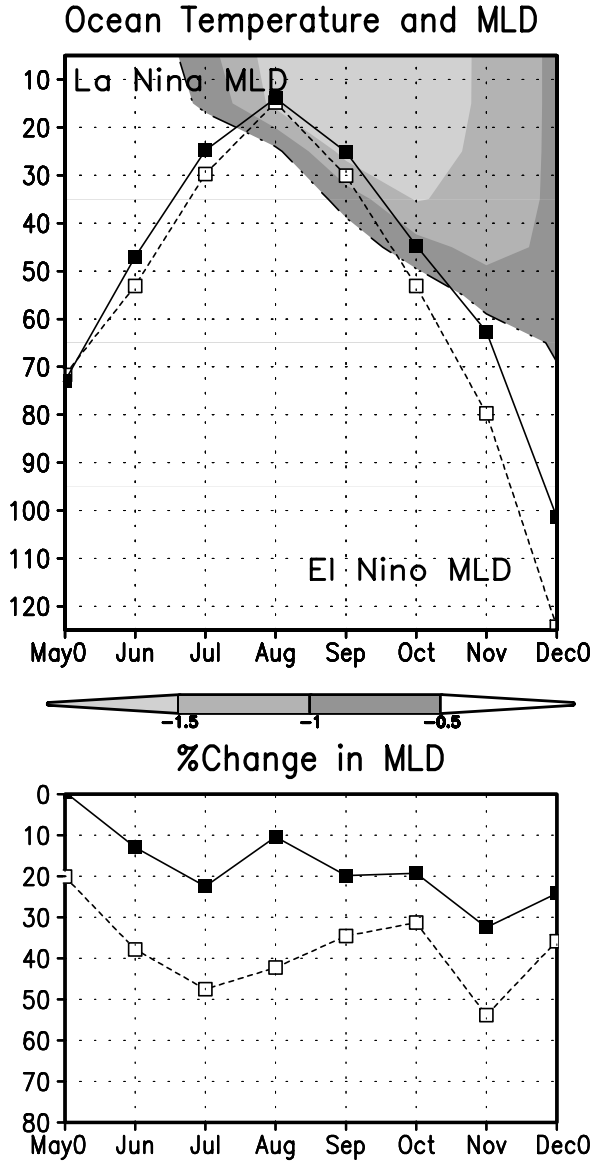


Figure 10. a) Composite El Niño – La Niña ocean temperature (shading, scale at bottom; values  $< -0.5^{\circ}\text{C}$  are enclosed by a dot-dash line) from May(0) to Dec(0) and the composite MLD (m) during El Niño (black squares) and La Niña (open squares) events in the western North Pacific region (see Figure 1). b) The percent change in the composite MLD during El Niño relative to La Niña events in the Western North Pacific region (black squares) and the north eastern portion of that region ( $170^{\circ}\text{E}-180^{\circ}$ ,  $39^{\circ}\text{N}-43^{\circ}\text{N}$ ; open squares). The temperatures are from the NCEP Ocean Analyses (Derber and Rosati, 1989; Ji et al., 1995) and the MLD from [White, 1995] for the period 1980-2001, the period when the ocean analyses are available.

Zhang et al. [1998] examined the seasonal persistence of North Pacific SST anomalies based on EOF and singular value decomposition (SVD) analyses. They found the

leading pattern in summer was similar to that in winter, but with the largest signal located along  $40^{\circ}\text{N}$  between  $160^{\circ}\text{E}-180^{\circ}$ , approximately  $30^{\circ}$  west of its wintertime position. In addition, the summer and winter patterns were highly correlated, which lead them to conclude that the SST anomalies persisted from one season to the next, possibly due to SST-stratus cloud interactions [Norris et al., 1998]. However, the leading EOF of North Pacific SSTs in summer and winter [Figures. 4 and 6 in Zhang et al., 1998] closely resemble the SST anomalies induced by the atmospheric bridge (Plate 1), including the westward displacement of the anomaly center in summer relative to winter. The rapid decorrelation time of summertime SST anomalies [Deser et al., 2003] and the strong relationship between tropical and North Pacific SST anomalies in all seasons, suggests that the connection between summer and winter SSTs in the North Pacific is not primarily due to local persistence, but rather to atmospheric forcing associated with ENSO, a conclusion reached by Newman et al. [2003] as well.

Once SST anomalies form in the North Pacific, they can influence the atmosphere both locally and perhaps remotely as well. The basic local atmospheric response to extratropical SST anomalies, is such that the near-surface air temperature and underlying ocean will adjust to each other, reducing the ocean-to-atmosphere damping of surface air temperature anomalies by  $Q_{sh}$ ,  $Q_{lh}$ , and  $Q_{lw}$ , which all depend on the air-sea temperature difference [e.g., Barsugli and Battisti, 1998; Bladé, 1999]. The effect of this “reduced thermal damping” is to enhance air temperature variance at interannual and longer time scales in coupled atmosphere-ocean models relative to atmospheric GCM simulations in which climatological SSTs are specified as boundary conditions.

An additional atmosphere-ocean interaction process in the North Pacific during summer involves positive feedbacks between stratus clouds and SSTs [e.g., Klein and Hartmann, 1993; and Norris and Leovy, 1994]. An increase in low clouds reduces  $Q_{sw}$  thereby cooling the SST, while colder SSTs enhance the static stability, which increases the strength of the surface inversion trapping the moisture that forms stratus clouds. In addition to the direct generation of clouds by atmospheric processes associated with storms, enhanced cloudiness over the North Pacific in summer may be due in part to the advection of warm air over cold SSTs in the regions of southerly flow between storms. Thus, the initial ENSO-driven increase in clouds and decrease in

SSTs over the northwest Pacific in summer may be enhanced by positive stratus cloud-SST feedbacks. Another local sea-air feedback involves the influence of static stability in the atmospheric boundary layer on vertical mixing of momentum. As the SST – air temperature difference increases, the static stability decreases, which enhances the vertical mixing of strong upper-level winds

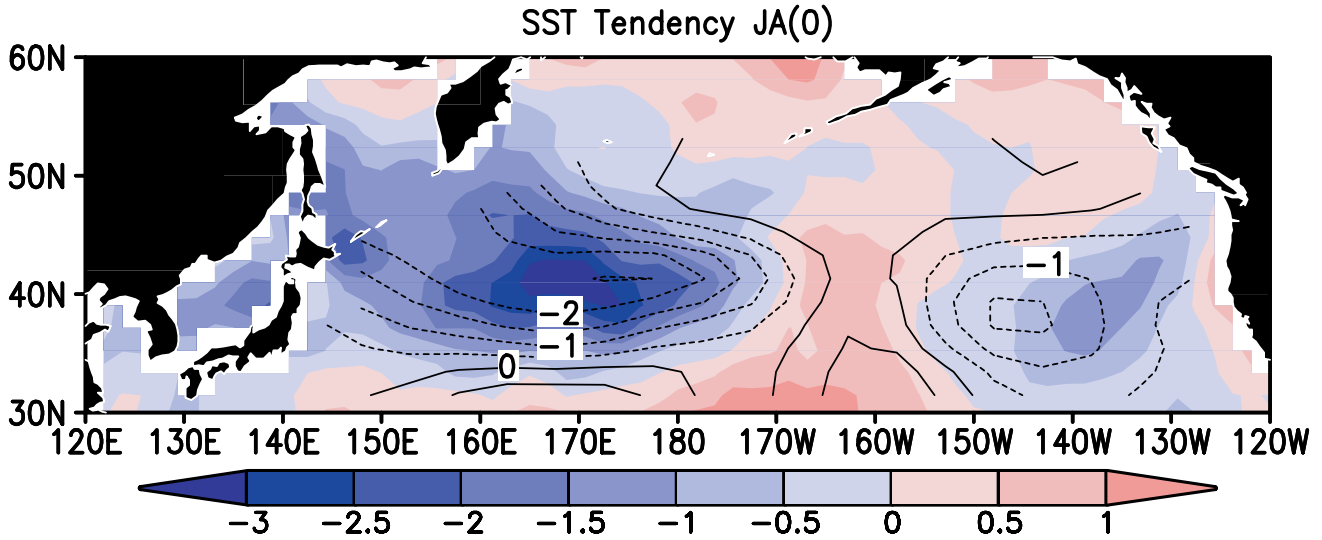


Plate 3. Composite El Niño – La Niña observed SST tendency and the SST tendency inferred from the net heat flux and Ekman transport ( $Q_e$ ) during JA(0) for ENSO events between 1983-2000. SST tendency is shaded and  $Q_e$  is contoured, both with an interval of  $0.5^\circ\text{C}$  over the 2 month period. The SST tendency is based on the difference in temperature between AS(0) and JJ(0). Both fields have been spatially smoothed using a 9-point filter.

down to the surface. Recent satellite data indicates, that while this process is strongest in winter, it also operates in the western North Pacific during summer [Nonaka and Xie, 2003]. Thus, surface wind speeds tend to be higher (lower) above warm (cold) SSTs, which would tend to reduce the wind speed in the WNP during El Niño events. The negative ENSO-related SST anomalies also enhance (reduce) the strong mean meridional SST gradient from  $140^\circ\text{E}$ - $180^\circ$  to the south (north) of  $\sim 40^\circ\text{N}$  (not shown). In regions where ocean temperature gradients are strong, SST-induced changes in static stability can influence the divergence and curl of the near-surface winds [Chelton *et al.*, 2001], which in turn can drive circulation changes beyond the boundary layer in both the atmosphere and ocean.

Several recent studies of extratropical atmosphere-ocean interaction in summer have investigated the relationships between, rainfall over Asia and/or North America, the large-scale atmospheric circulation and Pacific SST anomalies. Of the two leading patterns of precipitation and circulation variability, one involves a wave train that extends from eastern Asia to North America that is primarily associated with North Pacific SST anomalies, while the other resembles the ENSO-signal with zonally elongated height anomalies over the western North Pacific and SST anomalies of opposite sign in the tropical and North Pacific Ocean [Ting and Wang, 1997; Lau and Weng, 2002; Lau *et al.*, 2003]. Both patterns affect the North Pacific SST gradients, which in turn, may influence the near surface baroclinicity and thus the strength/position of the storm track and jet stream [Tanimoto *et al.*, 2003].

#### 4. CONCLUSIONS

While the atmospheric circulation anomalies associated with ENSO are strongest in boreal winter, significant SST anomalies develop outside the equatorial Pacific in summer soon after ENSO events begin, while others persist into the following summer, well after ENSO has dissipated. Here we have focused on two aspects of the remote atmosphere and ocean processes during ENSO: air-sea interaction in the tropical Indian and West Pacific Oceans over the seasonal cycle and the atmospheric bridge to the North Pacific in the summer of the ENSO year.

Anomalous cold (warm) water forms on the eastern (western) side of the tropical Indian Ocean, suggesting that ENSO contributes to the Indian Ocean SST dipole, the leading pattern of variability in boreal summer and fall. The eastern side of the basin warms rapidly in late fall and early winter resulting in positive SST anomalies across the entire Indian Ocean by the following spring. The SST anomalies in the tropical west Pacific also reverse sign, from negative in summer of Yr(0) to positive in the summer of Yr(1). The evolution of SST, SLP and precipitation anomalies shown here, and additional observational and modeling studies by Wang *et al.* [2003], Lau and Nath [2004] and Lau *et al.* [2004a], suggest that local air-sea interactions play an important role in the progression of ENSO-related anomalies over the tropical Indian and west Pacific Oceans. During the summer of Yr(0), the atmospheric response to ENSO includes a southward shift

in the Pacific storm track and jet stream, where the changes in synoptic eddy activity

appear to strongly influence the large-scale circulation. An increase in cloudiness along 40°N, to the west of the dateline, accompanies the bridge-induced circulation anomalies. While the atmospheric surface circulation anomalies are much weaker than in winter, SST anomalies can develop rapidly in the western North Pacific during summer as the solar radiation and latent heat flux anomalies are large and this surface forcing is integrated over the relatively shallow mixed layer. ENSO likely influences the large-scale upper-ocean variability in the North Pacific, as the bridge-related SST anomaly pattern in AS(0) is very similar to the leading EOF of SST poleward of 20°N in summer.

*Acknowledgements.* We thank Shiling Peng and Jeff Whitaker for their guidance in computing the eddy induced height tendency and Mary Jo Nath for her assistance in preparing several of the figures. We also thank Ileana Blade, Clara Deser, Dan Vimont and an anonymous reviewer for their suggestions that improved the manuscript. This work was supported in part by a grant from NOAA's CLIVAR-Pacific program.

#### REFERENCES

- Alexander, M. A., Midlatitude atmosphere-ocean interaction during El Niño. Part I: the North Pacific Ocean, *J. Climate*, 5, 944-958, 1992.
- Alexander, M. A., I. Bladé, M. Newman, J. R. Lanzante, N.-C. Lau, and J.D. Scott, The atmospheric bridge: the influence of ENSO teleconnections on air-sea interaction over the global oceans, *J. Climate*, 15, 2205-2231, 2002.
- Alexander, M. A., and J. D. Scott, The influence of ENSO on air-sea interaction in the Atlantic, 2002.
- Allan, R.J., D. Chambers, W. Drosowsky, H. Hendon, M. Latif, N. Nicholls, I. Smith, R. Stone, and Y. Yourre, Is there an Indian Ocean dipole, and is it independent of the El Niño-Southern Oscillation?, *CLIVAR Exch*, 6 (3), 18-22, 2001.
- Barlow, M., S. Nigam, and E.H. Berbery, ENSO, Pacific Decadal Variability, and U.S. Summertime Precipitation, Drought, and Stream Flow, *J. Climate*, 14, 2105-2128, 2001.
- Barnston, A. G., and R. E. Livezey, Classification, seasonality and persistence of low-frequency atmospheric circulation patterns, *Mon. Wea. Rev.*, 115, 1083-1126, 1987.
- Barsugli, J. J., and D. S. Battisti, The basic effects of atmosphere-ocean thermal coupling on midlatitude variability, *J. Atmos. Sci.*, 55 (4), 477-493, 1998.
- Behera, S. K., P. S. Salvekar, and T. Yamagata, Simulation of interannual SST Variability in the Tropical Indian Ocean, *J. Climate*, 13, 3487-3499, 2000.
- Bladé, I., The influence of midlatitude ocean-atmosphere coupling on the low-frequency variability of a GCM. Part II: Interannual variability induced by tropical SST forcing, *J. Climate*, 12, 21-45, 1999.
- Cadet, D. L., The Southern Oscillation over the Indian Ocean, *J. Climatol.*, 5, 189-212, 1985.
- Chambers, D. P., B. D. Tarpley, and R. H. Stewart, Anomalous warming in the Indian Ocean coincident with El Niño, *J. Geophys. Res.*, 104, 3035-3047, 1999.
- Chelton, D. B., and Coauthors, Observations of coupling between surface wind stress and sea surface temperature in the eastern tropical Pacific, *J. Climate*, 14, 1479-1498, 2001.
- Chen, T.-C., and M.-C. Yen, Interannual variation of summertime stationary eddies, *J. Climate*, 6, 2263-2277, 1993.
- Covey, D. L., and S. Hastenrath, The Pacific El Niño phenomenon in the Atlantic Sector, *Mon. Wea. Rev.*, 106, 1280-1287, 1978.
- Derber, J.D., and A. Rosati, A global oceanic data assimilation system, *J. Phys. Oceanogr.*, 19, 1333-1347, 1989.
- Deser, C., M. A. Alexander, and M. S. Timlin, Understanding the persistence of sea surface temperature anomalies in midlatitudes, *J. Climate*, 16 (1), 57-72, 2003.
- Enfield, D. B., and J. S. Allen, On the structure and dynamics of monthly mean sea level anomalies along the Pacific coast of North and South America, *J. Phys. Oceanogr.*, 10, 557-588, 1980.
- Frankignoul, C., Sea surface temperature anomalies, planetary waves, and air-sea feedback in the middle latitudes, *Rev. Geophys.*, 23, 357-390, 1985.
- Grimm, A. M., and P. L. Silva Dias, Analysis of tropical-extratropical interactions with influence functions of a barotropic model, *J. Atmos. Sci.*, 52, 3538-3555, 1995.
- Harrison, D. E., and N. K. Larkin, El Niño-Southern Oscillation sea surface temperature and wind anomalies, *Rev. of Geophys.*, 36, 353-399, 1998.
- Hendon, H. H., Indonesian rainfall variability: Impacts of ENSO and local air-sea interaction, *J. Climate*, 16, 1775-1790, 2003.
- Hoskins, B. J., and D. J. Karoly, The steady linear response of a spherical atmosphere to thermal and orographic forcing, *J. Atmos. Sci.*, 38, 1179-1196, 1981.
- Iizuka, S., and T. Matsura, The Indian Ocean SST dipole simulated in a coupled general circulation model, *Geophys. Res. Lett.*, 27, 3369-3372, 2000.
- Ji, M., A. Leetmaa, and J. Derber, An ocean analyses system for seasonal to interannual climate studies, *Mon. Wea. Rev.*, 123, 460-480, 1995.
- Kistler, R., E. Kalnay, W. Collins, S. Saha, G. White, J. Woollen, M. Chelliah, W. Ebisuzaki, M. Kanamitsu, V. Kousky, H. van den Dool, R. Jenne, and M. Fiorino, The NCEP-NCAR 50-Year Reanalysis: Monthly means CD-ROM and documentation, *Bull. Amer. Met. Soc.*, 82, 247-268, 2001.
- Klein, S. A., B. J. Soden, and N.-C. Lau, Remote sea surface variations during ENSO: evidence for a tropical atmospheric bridge, *J. Climate*, 12, 917-932, 1999.
- Klein, S.A., and D. L. Hartmann, The seasonal cycle of low stratiform clouds, *J. Climate*, 6, 1587-1606, 1993.
- Kok, C. J., and J. D. Opsteegh, Possible causes of anomalies in seasonal mean circulation patterns during the 1982-83 El Niño event, *J. Atmos. Sci.*, 42, 677-694, 1985.
- Kumar, A., and M. P. Hoerling, The nature and causes for the delayed atmospheric response to El Niño, *J. Climate*, 16, 1391-1403, 2003.
- Lau, K. M., K. M. Kim, I.-S. Kang and J. Y. Lee, The North Pacific as a regulator of summertime climate over Eurasia and North America, *J. Climate*, accepted, 2003.

- Lau, K.-M., and L. Peng, Dynamics of atmospheric teleconnections during the northern summer, *J. Climate*, *5*, 140-158, 1992.
- Lau, K.-M., and H. Weng, Recurrent teleconnection patterns linking summertime precipitation variability over east Asia and North America, *J. Meteor. Soc. Japan*, *80*, 1129-1147, 2002.
- Lau, N.-C., Variability of the observed midlatitude storm tracks in relation to low-frequency changes in the circulation pattern, *J. Atmos. Sci.*, *45*, 2718-2743, 1988.
- Lau, N.-C., and E. O. Holopainen, Transient eddy forcing of the time mean flow as identified by geopotential tendencies, *J. Atmos. Sci.*, *41*, 313-328, 1984.
- Lau, N.-C., and M. J. Nath, The role of the 'atmospheric bridge' in linking tropical Pacific ENSO events to extratropical SST anomalies, *J. Climate*, *9* (9), 2036-2057, 1996.
- Lau, N.-C., and M. J. Nath, Impact of ENSO on the variability of the Asian-Australian Monsoons as simulated in GCM experiments, *J. Climate*, *13* (24), 4287-4309, 2000.
- Lau, N.-C., and M.J. Nath, Atmosphere-ocean variations in the Indo-Pacific sector during ENSO episodes, *J. Climate*, *16*, 3-20, 2003.
- Lau, N.-C., and M. J. Nath, Coupled GCM simulation of atmosphere-ocean variability associated with zonally asymmetric SST changes in the tropical Indian Ocean, *J. Climate*, *17*, 245-265, 2004.
- Lau, N.-C., M. J. Nath, and H. Wang, Simulations by a GFDL GCM of ENSO-related variability of the coupled atmosphere-ocean system in the East Asian Monsoon region., in *East Asian Monsoon*, in press, World Scientific Publishing Company, 2004a.
- Lau, N.-C., A. Leetmaa, M. J. Nath, and H. Wang, Influences of ENSO-induced Indo-Western Pacific SST anomalies on extratropical atmospheric variability during the boreal summer, *J. Climate*, submitted, 2004b.
- Li, T., Y. Zhang, E. Liu, and D Wang, Relative role of dynamic and thermodynamic processes in the development of the Indian dipole: An OGCM diagnosis. *Geophys. Res. Lett.*, *29*, 2110, doi: 10.1029/2002GL015789.
- Li, T., B. Wang, C.-P. Chang, and Y. Zhang, A theory for the Indian Ocean dipole/zonal mode, *J. Atmos. Sci.*, *60*, 219-235, 2003.
- Luksch, U., and H. v. Storch, Modeling the low-frequency sea surface temperature variability in the North Pacific, *J. Climate*, *5*, 893-906, 1992.
- Meehl, G.A., The South Asian monsoon and the tropospheric biennial oscillation, *J. Climate*, *10*, 1921-1943, 1997.
- Mo, K.-C., J. R. Zimmerman, E. Kalnay, and M. Kanamitsu, A GCM study of the 1988 United States drought, *Mon. Wea. Rev.*, *119*, 1512-1532, 1991.
- Monterey, G. I., and S. Levitus, *Climatological Cycle of Mixed Layer Depth in the World Ocean*, 5 pp., 87 figs. pp., U.S. Gov. Printing Office, NOAA NESDIS, Wash., D.C, 1997.
- Murtugudde, R., J. P. McCreary, and A.J. Busalacchi, Oceanic processes associated with anomalous events in the Indian Ocean with relevance to 1997-1998, *J. Geophys. Res.*, *105*, 3295-3306, 2000.
- Newman, M., and P.D. Sardeshmukh, The impact of the annual cycle on the North Pacific/North American response to remote low frequency forcing, *J. Atmos. Sci.*, *55*, 1336-1353, 1998.
- Newman, M., G. P. Compo, and M. A. Alexander, ENSO-forced variability of the Pacific Decadal Oscillation, *J. Climate*, *16*, 3853-3857, 2003.
- Nicholson, S. E., An analysis of the ENSO signal in the tropical Atlantic and western Indian Oceans, *Int. J. Climatol.*, *17*, 345-375, 1997.
- Nitta, T., Convective activities in the tropical western Pacific and their impact on the Northern Hemisphere summer circulation, *J. Meteor. Soc. Japan*, *65*, 373-390, 1987.
- Nitta, T., Long term variations of cloud amount in the western Pacific region, *J. Meteor. Soc. Japan*, *64*, 373-390, 1986.
- Nonaka, M., and S.-P. Xie, Covariations of sea surface temperature and wind over the Kuroshio and its extension: Evidence for ocean-to-atmosphere feedback, *J. Climate*, *16*, 1404-1413, 2003.
- Norris, J. R., Interannual and interdecadal variability in the storm track, cloudiness, and sea surface temperature over the summertime North Pacific, *J. Climate*, *13* (2), 422-430, 2000.
- Norris, J. R., and C. Leovy, Interannual variability in stratiform cloudiness and sea surface temperature, *J. Climate*, *7*, 1915-1925, 1994.
- Norris, J. R., Y. Zhang, and J. M. Wallace, Role of clouds in summertime atmosphere-ocean interactions over the North Pacific, *J. Climate*, *11*, 2482-2490, 1998.
- Palmer, T. N., and C. Brankovic, The 1988 United States drought linked to anomalous sea-surface temperature, *Nature*, *338*, 54-57, 1989.
- Pares-Sierra, A., and J.J. O'Brien, The seasonal and interannual variability of the California Current System: a numerical model, *J. Geophys. Res.*, *94*, 3159-3180, 1989.
- Park, S., and C.B. Leovy, Marine cloud variations associated with ENSO, *J. Climate*, submitted, 2004.
- Rossow, W. B., and Y.-C. Zhang, Calculation of surface and top-of-atmosphere radiative fluxes from physical quantities based on ISCCP: Part II. Validation and first results, *J. Geophys. Res.*, *100*, 1167-1197, 1995.
- Saji, N. H., B. N. Goswami, P. N. Vinayachandran, and T. Yamagata, A dipole mode in the tropical Indian Ocean, *Nature*, *401*, 360-363, 1999.
- Saji, N. H., and T. Yamagata, Structure of SST and surface wind variability during Indian Ocean Dipole Mode events: COADS observations, *J. Climate*, *16*, 2735-2751, 2003.
- Schott, F. A., and J. P. McCreary, The monsoon circulation of the Indian Ocean, *Prog. Oceanogr.*, *51*, 1-123, 2001.
- Scott, J.D., and M.A. Alexander, Net shortwave fluxes over the ocean., *J. Phys. Oceanogr.*, *29*, 3167-3174, 1999.
- Shinoda, T., M.A. Alexander, and H.H. Hendon, Remote response of the Indian Ocean to interannual SST variations in the tropical Pacific, *J. Climate*, *17*, 362-372, 2004.
- Tanimoto, Y., H. Nakamura, T. Kagimoto, and S. Yamane, An active role of extratropical sea surface temperature anomalies in determining anomalous turbulent heat flux, *J. Geophys. Res.*, *108*(C10), doi:10.1029/2002JC001750, 2003.

- Ting, M. F. and N. C. Lau, A Diagnostic and Modeling Study of the Monthly Mean Wintertime Anomalies Appearing in a 100-Year GCM Experiment, *J. Atmos. Sci.*, 50, 2845-2867, 1993.
- Ting, M., and H. Wang, Summertime U.S. precipitation variability and its relation to Pacific sea surface temperature, *J. Climate*, 10, 1853-1873, 1997.
- Trenberth, K. E., and G. W. Branstator, Issues in establishing causes of the 1988 drought over North America, *J. Climate*, 5, 159-172, 1992.
- Trenberth, K. E., G. W. Branstator, and P. A. Arkin, Origins of the 1988 North American drought, *Science*, 242, 1640-1645, 1988.
- Trenberth, K. E., G. W. Branstator, D. Karoly, A. Kumar, N-C. Lau, and C. Ropelewski, Progress during TOGA in understanding and modeling global teleconnections associated with tropical sea surface temperatures., *J. Geophys. Res.*, 103, 14,291-14324, 1998.
- Venzke, S., M. Latif, and A. Villwock, The coupled GCM ECHO-2. Part II Indian Ocean response to ENSO, *J. Climate*, 13, 1384-1405, 2000.
- Wang, B., R. Wu, and T. Li, Atmosphere-warm ocean interaction and its impacts on the Asian-Australian monsoon variation, *J. Climate*, 16, 1195-1211, 2003.
- Wang, B., and Q. Zhang, Pacific-East Asian teleconnection. Part II: How the Philippine Sea anomalous anticyclone is established during El Niño development, *J. Climate*, 15, 3252-3265, 2002.
- Wang B., R. Wu, X. Fu, Pacific-East Asian teleconnection: How does ENSO affect East Asian climate?, *J. Climate*, 13, 1517-1536, 2000.
- Wang, C., Atmospheric circulation cells associated with the El Niño-Southern Oscillation, *J. Climate*, 15, 399-419, 2002.
- Wang, C., and J. Picaut, Understanding ENSO Physics – A Review, this volume.
- Weaver, C. P., and V. Ramanathan, The link between summertime cloud radiative forcing and extratropical cyclones in the North Pacific, *J. Climate*, 9 (9), 2093-2109, 1996.
- Webster, P. J., A. M. Moore, J. P. Loschnig, and R. R. Leben, Coupled ocean-atmosphere dynamics in the Indian Ocean during 1997-98, *Nature*, 401, 356-360, 1999.
- White, W. B., Design of a global observing system for gyre-scale upper ocean temperature variability, *Prog. Oceanogr.*, 36, 169-217, 1995.
- Wu, L., Q. Zhang, and Z. Liu, Toward understanding tropical Atlantic variability using coupled model surgery, this volume.
- Xie, P., and P. A. Arkin, Global precipitation: a 17-year monthly analysis based on gauge observations, satellite estimates, and numerical model outputs., *Bull. Amer. Meteor. Soc.*, 78, 2539-2558, 1997.
- Xie, S.-P., H. Annamalai, F. A. Schott, and J. P. McCreary, Structure and mechanisms of South Indian Ocean climate variability, *J. Climate*, 15, 864-878, 2002.
- Yamagata, T., S. K. Behera, J., J. Luo, S. Masson, M. R. Jury, and S. A. Rao, Coupled ocean-atmosphere variability in the tropical Indian Ocean, this volume.
- Yu, L., and M. M. Rienecker, Mechanisms for the Indian Ocean warming during the 1997-1998 El Niño, *Geophys. Res. Lett.*, 26, 735-738, 1999.
- Zhang, Y., J. R. Norris, and J. M. Wallace, Seasonality of large-scale atmosphere-ocean interaction over the North Pacific, *J. Climate*, 11, 2473-2481, 1998.
- Zhang, Y.-C., and W. B. Rossow, New ISCCP global radiative flux data products, <http://isccp.giss.nasa.gov/projects/flux.html>, 2004.
- Zhang, Y.-C., W. B. Rossow, and A.A. Lacis, Calculation of surface and top of atmosphere radiative fluxes from physical quantities based on ISCCP data sets. 1. Method and sensitivity to input data uncertainties, *J. Geophys. Res.*, 100, 1149-1165, 1995.

---

M. A. Alexander, National Oceanic and Atmospheric Administration – Cooperative Institute for Research in Environmental Sciences, Climate Diagnostics Center, R/CDC1, 325 Broadway, Boulder, CO 80305. Michael.Alexander@noaa.gov

N.-C. Lau, National Oceanic and Atmospheric Administration, Geophysical Fluid Dynamics Laboratory, Princeton University, P.O. Box 308, Princeton, NJ 08542. Gabriel.Lau@noaa.gov

J. D. Scott, National Oceanic and Atmospheric Administration – Cooperative Institute for Research in Environmental Sciences, Climate Diagnostics Center, R/CDC1, 325 Broadway, Boulder, CO 80305. James.D.Scott@noaa.gov